

## An intercomparison of AOD-converted PM<sub>2.5</sub> concentrations using different approaches for estimating aerosol vertical distribution

Tianning Su <sup>a</sup>, Jing Li <sup>b,\*</sup>, Chengcai Li <sup>b</sup>, Alexis Kai-Hon Lau <sup>c</sup>, Dongwei Yang <sup>b</sup>, Chuanyang Shen <sup>b</sup>

<sup>a</sup> Department of Atmospheric and Oceanic Sciences and Earth System Science Interdisciplinary Center, University of Maryland, College Park, MD 20740, USA

<sup>b</sup> Department of Atmospheric and Oceanic Sciences, Peking University, Beijing 100871, China

<sup>c</sup> Department of Civil and Environmental Engineering and Institute for the Environment, Hong Kong University of Science and Technology, Kowloon, Hong Kong



### HIGHLIGHTS

- Different approaches of calculating boundary layer heights are evaluated in retrieving surface PM<sub>2.5</sub> from AOD.
- Climatology pattern of aerosol vertical distribution constructed by lidar is proved to be effective for PM<sub>2.5</sub> remote sensing.
- The widely accepted assumptions in PM<sub>2.5</sub> remote sensing are examined.
- The elevated aerosols appear to be the major source of uncertainty for PM<sub>2.5</sub> remote sensing, especially for spring and summer.

### ARTICLE INFO

#### Article history:

Received 21 April 2017

Received in revised form

2 July 2017

Accepted 29 July 2017

Available online 1 August 2017

#### Keywords:

PM<sub>2.5</sub>

AOD

Aerosol vertical distribution

Boundary layer height

### ABSTRACT

Due to the limited spatial coverage of surface PM<sub>2.5</sub> monitoring sites, satellite AOD (aerosol optical depth) products have been widely used to estimate surface PM<sub>2.5</sub> in different parts of the world. A major difficulty as well as source of uncertainty in converting AOD to PM<sub>2.5</sub> is the determination of aerosol vertical distribution, usually represented by the boundary layer height (BLH). In this study, we evaluate the performance of different approaches of estimating aerosol vertical distributions in the AOD-PM<sub>2.5</sub> conversion process, using long-term and multi-source data acquired at a super station, Yuen Long, Hong Kong. The monthly climatology of aerosol vertical distribution and BLH products derived from lidar, radiosonde, and MERRA reanalysis data are respectively applied for converting AOD to surface aerosol extinction coefficients. Seasonal empirical hygroscopic growth functions are constructed to convert aerosol extinction to dry PM<sub>2.5</sub> mass concentration. Results indicate that different vertical distribution estimation approaches can have highly varying effect on the converted PM<sub>2.5</sub> concentration. Using lidar-derived BLHs shows the best agreement, with a correlation coefficient of 0.73 and a relative bias of 30.6% between retrievals and observations. Since continuous lidar measurements are not available for most regions, the climatology pattern of aerosol structure and radiosonde-derived BLHs are found to be suitable alternatives with a correlation coefficient of ~0.6, and considerably outperform the results using BLHs derived from reanalysis data. Elevated aerosol layers appear to be the major source of uncertainty and result in an overestimate of satellite results, especially during the spring and summer seasons.

© 2017 Elsevier Ltd. All rights reserved.

### 1. Introduction

PM<sub>2.5</sub> (particulate matter with an aerodynamic diameter smaller than 2.5 μm) is an official indicator to represent fine particle

abundance, and has severe impact on the environment and human health (Brunekreef and Forsberg, 2005; Dockery et al., 1993; Engel-Cox et al., 2013), as well as on the Earth's climate through aerosol direct and indirect effects (Boucher et al., 2013; Kiehl and Briegleb, 1993; Ackerman et al., 2004; Guo et al., 2017). In the past three decades, China has been suffering from an increasingly severe particulate matter pollution problem, and this issue together with its causes have attracted extensive attention (Chan and Yao, 2008; J.

\* Corresponding author.

E-mail address: [jing-li@pku.edu.cn](mailto:jing-li@pku.edu.cn) (J. Li).

Li et al., 2016; Su et al., 2017a). Realizing the importance of monitoring PM<sub>2.5</sub> in the atmosphere, real-time gravimetric measurements of PM<sub>2.5</sub> are widely implemented by the Chinese Ministry of Environmental Protection for surface monitoring since 2013. Nevertheless, there is still a lack of historical measurements, and spatial coverage for in situ observation is limited. As an alternative method, PM<sub>2.5</sub> can be estimated through satellite-based remotely sensing, which has been investigated and applied to various environmental studies (C. Q. Lin et al., 2016; Lu et al., 2017; Li et al., 2015). In particular, advanced sensors such as the MODerate resolution Imaging Spectroradiometer (MODIS) are capable of deriving long-term aerosol optical depth (AOD) measurements on global scale. Many researchers have used MODIS AOD products to derive surface PM (Particulate matter) concentrations (e.g., van Donkelaar et al., 2006; Lee et al., 2011; Wang et al., 2010; Lin et al., 2015; Karimian et al., 2016; Wu et al., 2012).

Since AOD characterizes the columnar integration of aerosol extinction coefficients while PM<sub>2.5</sub> represents the surface mass concentration of aerosols, the aerosol vertical distribution is a key issue in the conversion processes. A number of previous studies used aerosol vertical structure simulated by global or regional chemical transport models (e.g. Drury et al., 2010; Liu et al., 2004). These approaches have the advantage of generating real time spatial PM<sub>2.5</sub> map (van Donkelaar et al., 2012), but are limited by the numerical model's various sources of uncertainties (Carlton et al., 2009; Zheng et al., 2009). Apart from modeling, empirical statistical regression based on observations were also used to establish the relationship between AOD and surface PM, ranging from simple linear regressions to complex multi-variable regressions (e.g., against boundary layer height, temperature, relative humidity, and wind) (Chu et al., 2003; Wang and Christopher, 2003; Benas et al., 2013; Li et al., 2011; Guo et al., 2009). Since planetary boundary layer (PBL) exerts significant impacts on the aerosol vertical structure with the bulk of pollutants concentrated within this layer, the boundary layer height (BLH) is a critical parameter that is widely used to characterize aerosol vertical distributions in multiple studies (Schäfer et al., 2008; Boyouk et al., 2010; Barnaba et al., 2010). Under such estimations, aerosols are

usually assumed to be vertically confined by the top of boundary layer, and homogenously mixed within this layer. These assumptions are referred to as “confinement assumption” and “homogenous assumption” respectively in the following analysis. Since BLH is a diagnostic parameter, BLH derived from various sources have been utilized to retrieve PM<sub>2.5</sub>, such as lidar (Wang et al., 2014; Z. Li et al., 2016), reanalysis data (Zhang and Li, 2015), radiosonde (RS) (Chu et al., 2015), and surface meteorology parameters (He et al., 2016).

It should be noted that considerable differences can be introduced in deriving the BLH, depending upon the definition, the physical parameter and the observation technique used (Seibert et al., 2000; Wiegner et al., 2006; Su et al., 2017b). As a result, estimation of surface PM mass concentration based on BLH obtained from different sources will inevitably yield different results. However, previous studies typically rely on a single method to calculate the BLH. It is thus necessary to systematically compare and evaluate the performance of different BLH retrieving approaches in converting columnar AOD to surface PM concentrations. Moreover, the confinement and homogenous assumptions made in estimating aerosol vertical distribution by the BLH may also result in uncertainties, whose effect is yet to be examined, although they are usually taken as granted by previous studies.

Based on the shortcomings mentioned above, this study aims to evaluate several typical observation-based approaches for estimating aerosol vertical distribution in the retrieval of PM<sub>2.5</sub> using satellite AOD, through a detailed examination of the retrieval process. The techniques for retrieving BLHs considered include micro-pulse lidar (MPL), radiosondes (RS) and reanalysis data. We also originally apply a method based on the monthly climatology of aerosol vertical distribution in retrieving PM<sub>2.5</sub>. Moreover, the seasonal hygroscopic growth functions are constructed to correct the effects of humidity. The study is conducted at a super observation site in Hong Kong, named Yuen Long, where long-term multi-source data is available.

The paper proceeds as follows: Section 2 introduces the datasets used and the methods for deriving aerosol extinction coefficients and BLHs. The detailed assessment of the retrieval processes is presented in Section 3, and the intercomparison of satellite retrievals derived from different approaches is presented in section 4. Section 5 discusses the results with a brief conclusion.

## 2. Data and method

### 2.1. Sites description

The Yuen Long station (114.02°E, 22.44°N, blue square in Fig. 1) is a meteorological station located at the northwest of Hong Kong. Intense meteorological and environmental observations are routinely carried out at this station. In this study, we utilize surface measurements of relative humidity (RH), PM<sub>2.5</sub>, visibility, as well as MPL-based extinction profiles measured here. The RS measurement is available at 0 800/2000 China standard time (CST) at the RS station of Hong Kong (red triangle in Fig. 1). Hong Kong is a megacity located at the Pearl River Delta of China, and is one of the most densely populated and well urbanized regions in the world. Due to the rapid economic development and industrialization of the Pearl River Delta, Hong Kong has been faced with a serious air quality issue (Li et al., 2015).

The MPL located at the YL station is a SESI (Science and Engineering Services, Inc.) MODEL 1 000 manufactured by the SESI Corporation, and was continuously operated with a temporal resolution of 15s and a vertical resolution of 30 m, and at a wavelength of 523.5 nm, from 2004 to 2009. This MPL stopped working because of facility malfunction since January 2010. Due to incomplete laser

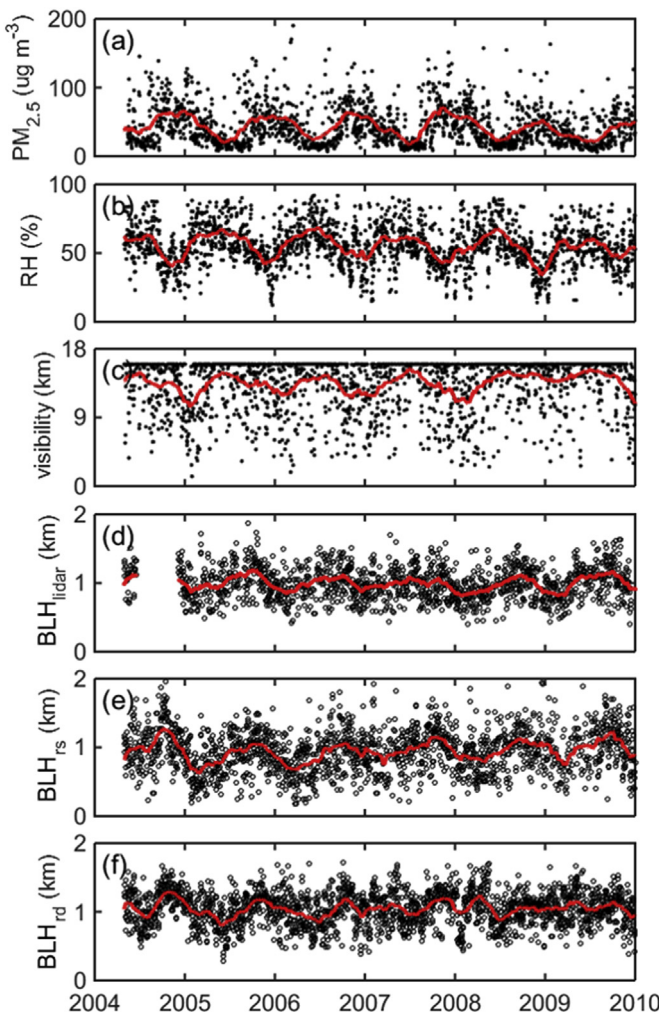


Fig. 1. Locations of Yuen Long (blue square) and radiosonde (RS, red triangle) stations.

pulses, there is a 130 m blind zone for the MPL. A Belfort Model 6 000 visibility sensor is collocated with the MPL, which measures visibility using 550 nm forward scatter. The upper limit of visibility is set to ~16 km, and the measurements above this upper limit are excluded from the following analysis. The mass concentration of  $\text{PM}_{2.5}$  is continuously measured using a tapered element oscillating microbalance (TEOM). The RH is obtained from an automatic weather station manufactured by Vaisala Ltd. The time series of noontime  $\text{PM}_{2.5}$ , RH, and visibility are presented in Fig. 2a, b, c. Here and in the following analysis, the “noontime” refers to results averaged from 1 100 to 1 400 CST, the major period of interest for this study.

## 2.2. MODIS AOD data

NASA's EOS polar-orbiting satellites, Terra and Aqua, are in 705-km Sun-synchronous polar orbits between 82°N and 82°S, with equator crossings at approximately 10:30 and 13:30 local time, respectively. The MODIS instrument onboard Terra and Aqua has a 2 330-km swath width, and provides daily AOD data with near global coverage. In this study, we use Collection 6 products of MODIS level-2 AOD at 550 nm that are publicly available online



**Fig. 2.** Time series of noontime  $\text{PM}_{2.5}$  (a), RH (b), visibility (c),  $\text{BLH}_{\text{lidar}}$  (d),  $\text{BLH}_{\text{rs}}$  (e), and  $\text{BLH}_{\text{rd}}$  (f).  $\text{PM}_{2.5}$ , RH, and visibility are measured from the surface instruments at Yuen Long station, while  $\text{BLH}_{\text{lidar}}$ ,  $\text{BLH}_{\text{rs}}$ , and  $\text{BLH}_{\text{rd}}$  represent the boundary layer height (BLH) derived from lidar, radiosonde, and reanalysis data respectively. The red lines indicate 70-day running mean for these time series.

from the Atmospheric Science Data Center at NASA Langley Research Center (<https://www.nasa.gov/langley>). The data are archived with a nominal spatial resolution of 10 km × 10 km. For acquiring AOD at the Yuen Long station, MODIS AOD data are averaged within 20 km radius around the Yuen Long station. The MODIS land AOD accuracy is reported to be  $\pm(0.05 + 15\% \text{ AERONET AOD})$  (Levy et al., 2010). Previous studies have validated the MODIS AOD by ground-based solar photometer over Hong Kong, and achieved a correlation coefficient above 0.9 (Li et al., 2003, 2005a; C. Q. Lin et al., 2016; Tao et al., 2015).

## 2.3. Retrieving aerosol extinction coefficient profile using MPL

Multiple studies have provided a well-established algorithm to retrieve the vertical profiles of aerosol extinction coefficient from MPL (eg., Fernald, 1984; Klett, 1985; Campbell et al., 2013). Hereafter, we simply refer the aerosol extinction coefficient as “extinction”. We first process the raw data by background subtraction, saturation, afterpulse, overlap and range corrections, and exclude the cloudy conditions using the threshold method (Platt et al., 1994; Yang et al., 2013). Then, the Klett method is further applied for retrieving extinction profiles (Klett, 1985). The column-averaged extinction-to-backscatter ratio (so-called lidar ratio) is an important parameter in the retrieval processes, and is usually constrained using the ground-based AOD observation (e.g. sunphotometer). Nonetheless, due to the lack of continuous ground-based AOD measurements at the lidar site, an alternative method for estimating lidar ratio proposed by He et al. (2006) is applied to constrain lidar ratio by collocated MODIS AOD. Linear interpolation is performed between different values of lidar ratio throughout the entire study period. The overall uncertainties from overlap function, lidar ratio, effects of multiple scattering, and noises are estimated to fall within a range of 20–30% in the retrieval processes (He et al., 2006).

## 2.4. Retrieving BLHs

### 2.4.1. BLHs derived from micropulse lidar

There are a variety of methods for retrieving BLH from MPL, such as visual inspection (Boers et al., 1984), signal threshold (Melfi et al., 1985), minimum of derivative of signal profile (Flamant et al., 1997), maximum of signal variance (Hooper and Eloranta, 1986), wavelet transform (Cohn and Angevine, 2000), etc. In this study, we adopt the well-established method by Yang et al. (2013) to derive BLH from MPL data, with a few modifications. This method is based on the idea of maximum gradient. Briefly, Yang et al. (2013) applied the first derivative of a Gaussian filter with a wavelet dilation of 60 m to smooth the vertical profile of MPL signals, and to produce the gradient profile. The stratification structure of aerosols is identified by multiple valleys and peaks of the gradient profile. For excluding the misidentification due to elevated aerosol layers above the PBL, the first significant peak (if exists) in the gradient profile is considered as the upper limit for searching the PBL top. Then the height of the deepest valley of the gradient profile would be attributed as the BLH, and the false results caused by clouds are subsequently eliminated. A manual quality assurance is further applied for adjusting some erroneous results.

In this study, we automate the above process with several modifications. Following Morille et al. (2007), we estimate the shot noise ( $\sigma$ ) induced by background light and dark current for a single profile, and then added threshold values of  $\pm 3\sigma$  for the identified peaks and valleys of this profile to exclude the effects of noises. In addition, to avoid any subjective bias, we eliminate the manual quality assurance step.

#### 2.4.2. BLHs derived from radiosondes

Since RS is only launched twice daily, to obtain noontime BLH, we apply the method proposed by Holzworth, (1964, 1967) to obtain diurnally varying BLHs using morning potential temperature profile and daily surface potential temperature. Briefly, along with the increase of surface temperature from the morning, the air mass is assumed to be lifted adiabatically from the surface to higher altitudes with a nearly constant potential temperature. The BLH refers to the height at which the environment potential temperature and current surface potential temperature reach equilibrium. Conventionally, the environment potential temperature profile is measured by the radiosonde launched at 0 800 CST at the RS station, and the diurnal variability of surface potential temperature is determined by the hourly surface potential temperatures obtained from the automatic weather station at the Yuen Long station. In the Holzworth method, the potential temperature is assumed to be constant for the same day at the same altitude of the free atmosphere, and the potential temperature is assumed to be homogenous within the PBL. Although these assumptions might introduce some uncertainties, the Holzworth method is a practical method for estimating BLH, and is widely used by a range of studies (e.g., Du et al., 2013; Zhang et al., 2014; Lai, 2015; Karimian et al., 2016).

#### 2.4.3. BLHs obtained from MERRA

Reanalysis datasets can also provide BLH on an hourly basis. In this study, we use the BLH data from the Modern Era-Retrospective Reanalysis for Research and Applications (MERRA) reanalysis dataset (Rienecker et al., 2008, 2011). The MERRA reanalysis data uses a new version of the Goddard Earth Observing System Data Assimilation System Version 5 (GEOS-5), which is a state of the art system coupling a global atmospheric general circulation model (GEOS-5 AGCM) to NCEP's Grid-point Statistical Interpolation (GSI) analysis. The GEOS-5 BLH data used for this study is hourly averaged with a spatial resolution of  $2/3 \times 1/2^\circ$  (longitude-latitude). We acquire the MERRA-BLHs at Yuen Long from the grid containing this station. Comparing with other products (e.g., ECMWF), MERRA-BLHs have relatively high temporal and spatial resolutions, and are widely applied in multiple research works (e.g., Jordan et al., 2010; McGrath-Spangler and Denning., 2012; Kennedy et al., 2011; Sayer et al., 2016).

In total, we introduce three independent BLH results from MPL, RS, and MERRA reanalysis data, which are referred to as  $BLH_{lidar}$ ,  $BLH_{rs}$ , and  $BLH_{rd}$  respectively. The time series of noontime  $BLH_{lidar}$ ,  $BLH_{rs}$ , and  $BLH_{rd}$  are presented in Fig. 2d, e, f. It can be seen that there are distinct and similar seasonality and inter-annual variations for  $BLH_{lidar}$  and  $BLH_{rs}$ , whereas the time evolution of  $BLH_{rd}$  is relatively irregular.

### 3. Assessment of the retrieval processes of AOD-converted $PM_{2.5}$

Following previous studies, we retrieve  $PM_{2.5}$  from AOD through vertical and humidity corrections (Li et al., 2005b; Wang et al., 2010). For the first step, the columnar AOD is converted to the surface extinction by applying different approaches for estimating vertical distribution. Then the surface extinction is transformed to  $PM_{2.5}$  by empirical hygroscopic functions. In this section, we focus on the evaluation of these processes with a special interest in the intercomparison of different approaches for vertical distributions.

#### 3.1. Converting columnar AOD to surface extinction

First, we apply the different approaches to estimate aerosol

vertical distribution, and convert the columnar AOD to surface extinction. Based on the method of retrieving vertical distribution of aerosol extinction described in Section 2.3, Fig. 3 presented the monthly averaged profiles of noontime extinction derived from the MPL data during 2004–2009, with positions of monthly mean noontime  $BLH_{lidar}$ ,  $BLH_{rs}$ , and  $BLH_{rd}$  marked by dashed lines. Generally, the monthly mean positions of  $BLH_{lidar}$  and  $BLH_{rs}$  are similar, and both agree well with the vertical extent of aerosols. Monthly mean  $BLH_{rd}$  also resembles  $BLH_{lidar}$  and  $BLH_{rs}$  in summer and autumn, whereas it yields higher values in spring and winter. Monthly mean extinction profiles reach maxima near the top of the PBL, and decrease exponentially above the PBL. In general, the bulk of aerosols are confined within the lowest 1.5 km, and the aerosol concentration decreases from January to June and then increases from July to December. By utilizing the climatology pattern of extinction profiles, the monthly mean ratios between surface extinction and AOD can be calculated, which are marked in each panel of Fig. 3.

Based on the noontime extinction profiles derived from the MPL, we calculate the AOD and surface extinction. Due to the blind zone, surface extinction is calculated as the extinction at 130 m, and that below 130 m is assumed to be equal to surface value. Fig. 4a presents the seasonal correlations between AOD and surface extinction, from which we can see that the correlations are lower for spring and summer. Since the climatology pattern of vertical distribution of noontime extinction was constructed, we can obtain monthly linear relationships between surface extinction and columnar AOD using the following equation:

$$\text{estimated } \sigma_a = \text{AOD} \cdot \gamma(M) \quad (1)$$

where M represents month, and  $\gamma(M)$  indicates the monthly linear relationships between surface extinction and AOD (c.f., Fig. 3). This relationship can thus be used to convert AOD to surface extinction (referred to as "estimated surface extinction").

Fig. 4b compares the estimated extinction using Eq. (1) with the observed values. After applying monthly climatology pattern of aerosol vertical distributions, the correlations are improved for each season and all.

Another method for estimating aerosol vertical distribution is by utilizing BLH. Previous studies generally assumed that aerosols are vertically confined by the top of boundary layer, and are homogeneously mixed in this layer (e.g., Boyouk et al., 2010; Zhang and Li, 2015; Z. Li et al., 2016). Therefore, under the confinement and homogenous assumptions, surface extinction should equal to the ratio between AOD and BLH.

Based on this idea, Fig. 5 shows the seasonal comparison of noontime surface extinctions and  $\frac{\text{AOD}}{\text{BLH}}$ , where  $BLH_{lidar}$ ,  $BLH_{rs}$ , and  $BLH_{rd}$  serve as input parameters respectively. Similar to the correlation between AOD and surface extinctions, the correlations between surface extinctions and  $\frac{\text{AOD}}{\text{BLH}}$  are lower in spring and summer. The correlation is also found to be considerably higher for  $BLH_{lidar}$ . Moreover, we found that  $\frac{\text{AOD}}{\text{BLH}}$  has an overall high bias against surface extinction, implying potential errors in the two assumptions. Therefore, we further calculated the ratio (refers as " $\alpha$ ") of AOD above the BLH and total AOD, and Fig. 6a presented the seasonal distributions of  $\alpha$  calculated from  $BLH_{lidar}$ ,  $BLH_{rs}$ , and  $BLH_{rd}$  respectively. It is found that the values of  $\alpha$  are quite high, and even reaches above 0.5 in spring. This indicates that a large fraction of columnar AOD is attributed to the aerosols above the PBL, contrary to the assumption that all aerosols are within the PBL. On the other hand, the comparisons between surface extinction and mean extinction within the BLH show good agreements (Fig. 6b–d),

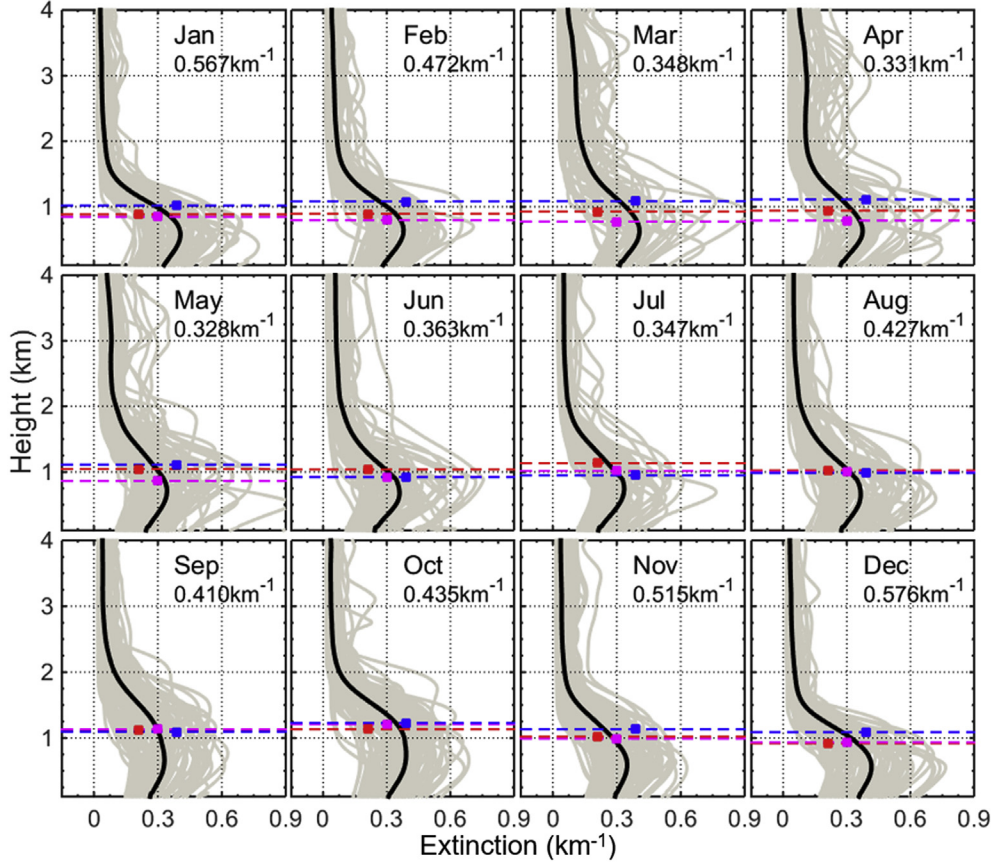


**Fig. 3.** The monthly climatology pattern of the vertical distribution of noontime extinction at Yuen Long during the study period. Black lines represent the monthly mean, while individual observations in each day are plotted as gray lines. The red, pink, and blue dashed lines represent the monthly means of noontime  $BLH_{lidar}$ ,  $BLH_{rs}$ , and  $BLH_{rd}$ . The monthly mean ratios ( $\gamma(M)$ ) between surface extinction and AOD are given in each panel of Fig. 3.

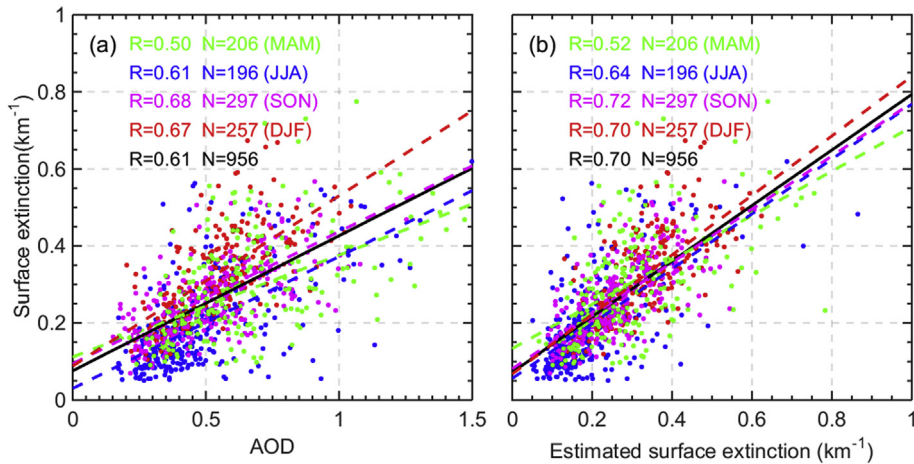


**Fig. 4.** (a) Comparison between the noontime surface extinction and AOD for MAM (green, spring), JJA (blue, summer), SON (pink, autumn), DJF (red, winter). Surface extinction and AOD are both calculated from lidar's extinction profiles. (b) Comparison between the observed surface extinction and estimated surface extinction derived from AOD along with the climatology pattern of aerosol vertical distribution. The correlation coefficients (R) and sample numbers (N) for each season and total (black) are given in each panel.

which verifies that the aerosols are indeed well mixed in the PBL. Therefore, the major source of uncertainty in retrieving surface extinction through BLH appears to come from the confinement assumption, in particular, the elevated aerosols above the PBL.  $\alpha$  is found to have larger ranges of variability in spring and summer, which agrees well with the lower correlations for these two seasons in Fig. 5. To avoid the bias associated with aerosols above the

PBL, we further introduce a constant  $\varepsilon$  in retrieving surface extinction, and Eq. (1) is now updated as:

$$\text{estimated surface extinction} = \frac{AOD_{PBL}}{BLH} = (1 - \alpha) \cdot \frac{AOD}{BLH} \quad (2)$$

where  $AOD_{PBL}$  represents the AOD within PBL,  $\alpha$  indicates the ratio

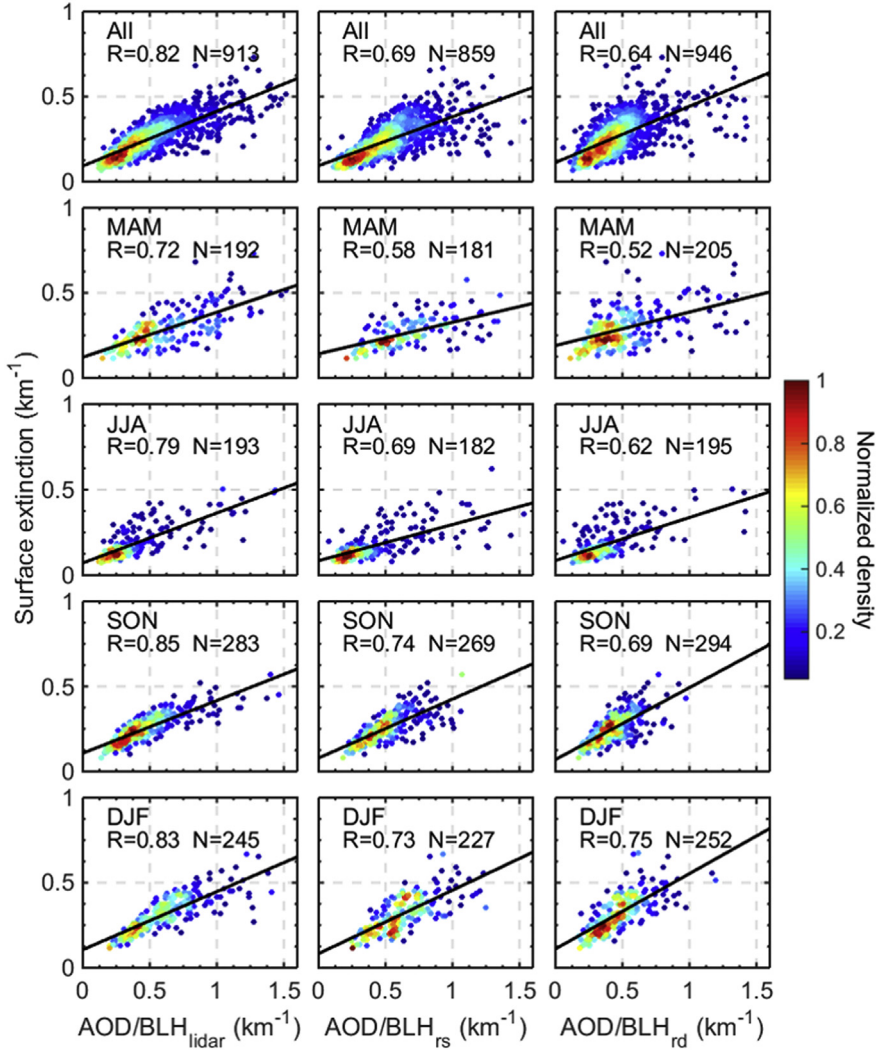


**Fig. 5.** Seasonal comparison of noontime surface extinction and  $\frac{\text{AOD}}{\text{BLH}}$ . Three approaches for BLH are applied to the correlation respectively. The color-shaded dots indicate the normalized sample density.

of AOD above the BLH to the total AOD. Since there are differences between different BLH approaches,  $\alpha$  are approximated as 0.43, 0.46, and 0.40 for  $BLH_{lidar}$ ,  $BLH_{rs}$ , and  $BLH_{rd}$  respectively, using annual statistics. Following Eq. (1) and Eq. (2), we have presented four approaches for converting AOD to surface extinctions, noting that Eq. (2) involves BLH estimated using three methods.

### 3.2. Correction for hygroscopic growth

In addition to the correction for aerosol vertical distribution, other important factors must be taken into account. Following the previously well-established algorithm (Koelemeijer et al., 2006; Zhang and Li, 2015), mass concentration of  $PM_{2.5}$  can be estimated by extinction from the following equation:

$$PM_{2.5} = \frac{FMF}{\frac{3(Q_{ext})}{4r_{eff}} \cdot f(RH)} \cdot extinction = \frac{FMF}{\alpha_{ext} \cdot f(RH)} \cdot extinction \quad (3)$$

where FMF represents fine mode fraction,  $Q_{ext}$  denotes the size-distribution integrated extinction efficiency,  $r_{eff}$  is the effective radius,  $\rho$  is the aerosol mass density,  $\alpha_{ext}$  indicates the mass extinction efficiency of the aerosol mixtures, and  $f(RH)$  is the

hygroscopic growth factor.

Because aerosol properties themselves may also vary with relative humidity, we follow the previous approach by Lin et al. (2015) and modify Eq. (3) as an empirical fitting function to characterize the relationship between ambient aerosol extinction and  $PM_{2.5}$ :

$$G = \frac{\alpha_{ext} \cdot f(RH)}{FMF} = \frac{A}{(100 - RH)^{\lambda}} \quad (4)$$

where the  $G$  and  $A$  have units  $m^2 g^{-1}$ , the unit of RH is set as %, and  $\lambda$  has arbitrary unit. The parameters  $A$  and  $\lambda$  are to be determined by non-linear least square fitting. We notice that the fitted  $G$ -RH relationship bares similar behavior to the hygroscopic growth factor  $f(RH)$ , both showing nonlinear increase with RH.

For investigating the integrated relationship between  $G$  and RH, we present the hourly-averaged ratio between extinction and mass concentration of  $PM_{2.5}$  for all four seasons in Fig. 7. In order to guarantee continuity and sufficient sampling, the extinction is not derived from lidar measurements but is derived from surface visibility as 3.912/visibility (Koschmieder, 1926). Following Eq. (4), the corresponding fitting curves are plotted in Fig. 7, and the specific

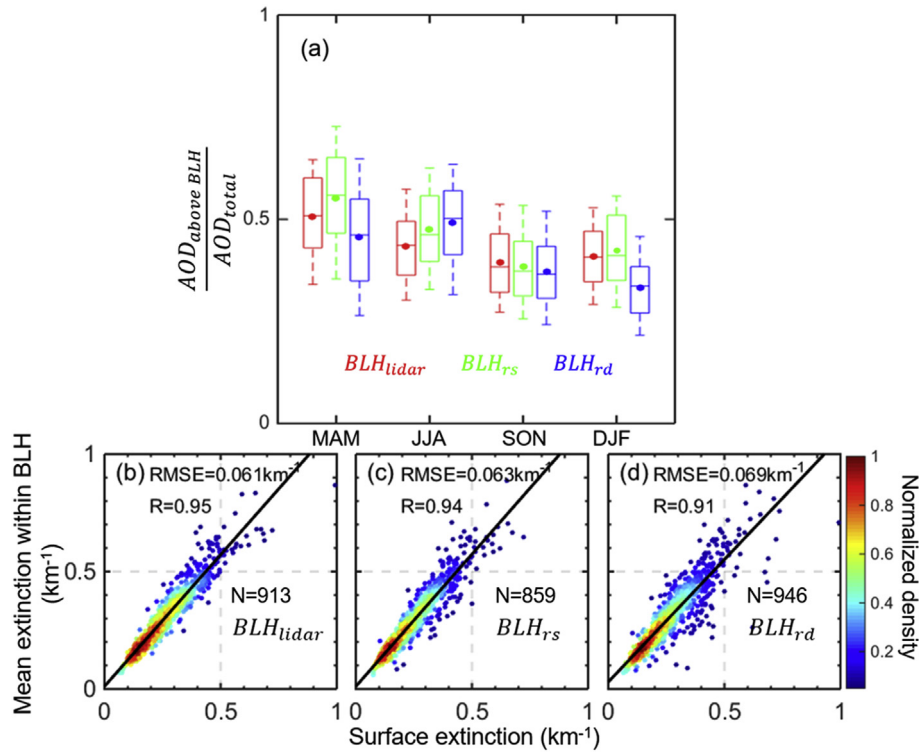


**Fig. 6.** (a) Seasonal box-and-whisker plots showing the 10th, 25th, 50th, 75th, and 90th percentile values of the ratio between AOD above BLH and total AOD.  $BLH_{\text{lidar}}$  (red),  $BLH_{\text{rs}}$  (green), and  $BLH_{\text{rd}}$  (blue) are applied to calculate the AOD above BLH respectively. The dots indicate the mean value for each approach. The comparisons between surface extinction and mean extinction within the PBL, with the BLHs calculated using (b)  $BLH_{\text{lidar}}$ , (c)  $BLH_{\text{rs}}$ , and (d)  $BLH_{\text{rd}}$  respectively.

functions are given in each panel. In general,  $G$  slowly grows for a RH range of 20%–70%, and then sharply increases at high RH (>70%).

We can see that over Hong Kong, high RH is more frequently

observed in spring and summer, when relatively large deviations between observations and the fitting curves are observed as well. When RH is above 90%, the function  $G(RH)$  grows much faster and results in larger errors, and these cases are subsequently eliminated

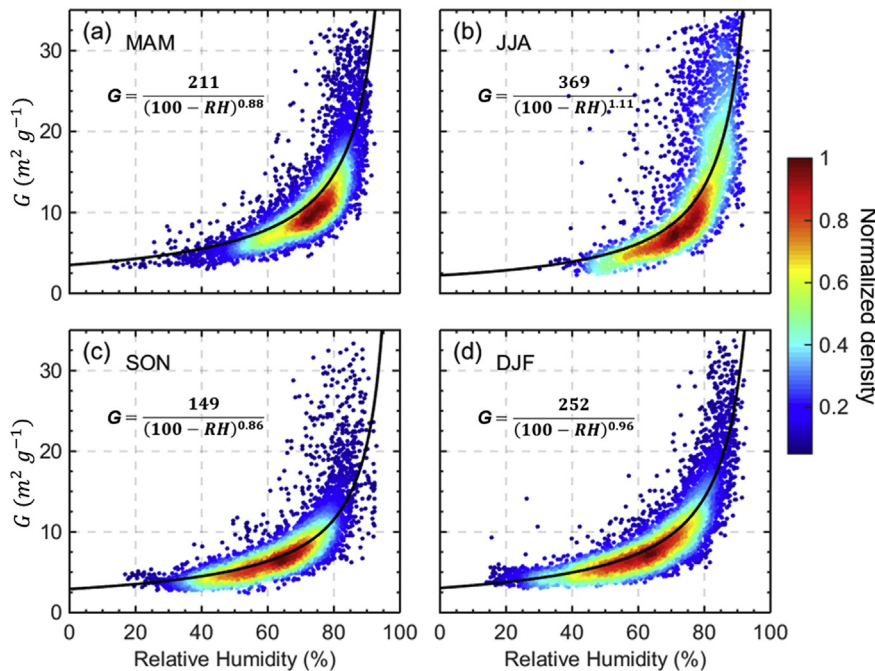


**Fig. 7.** Dependence of the function  $G$  on RH for (a) MAM, (b) JJA, (c) SON, and (d) DJF. The color-shaded dots indicate the normalized sample density. The black lines indicate the fitting curves, and the specific functions are given on each panel.

in the following analysis. The function  $G(RH)$  highly depends on the mass scattering extinction efficiency for different types of aerosols. The different fitting curves during different seasons are caused by the seasonal differences in the chemical compositions and source attribution of aerosols over Hong Kong. Moreover, it should be noted that  $G$  not only depends on the mass scattering extinction efficiency, but is also related to the particle size. Particles larger than  $PM_{2.5}$ , such as dust, would contribute to extinction, but wouldn't increase the concentration of  $PM_{2.5}$ . Nonetheless, the surface pollutants in Hong Kong are dominated by fine particles caused by industrial emissions and automobile exhausts (Qin et al., 2016; Ho et al., 2006). Therefore, the size issue is not significant in this study.

Accounting for the RH effect, the mass concentration of  $PM_{2.5}$  can be estimated by Eq. (5):

$$\text{estimated } PM_{2.5} = \text{extinction}/G(RH) \quad (5)$$

where the functions  $G$  are considered to vary from season to season. Then, we apply the pre-described fitting curves for each season to the noontime surface extinction derived from the MPL, and the corresponding comparisons are presented in Fig. 8. The correlations are significantly improved for each season and as a whole by applying humidity correction, which further validate the effectiveness of the fitting curves. Meanwhile, the correlation coefficients between  $PM_{2.5}$  and extinction/ $G$  are also relatively low for spring and summer, consistent with the large deviations between observations and fitting curves in Fig. 7 for these two seasons. This phenomenon may be caused by the more complex chemical composition in spring and summer due to the transport from inland.

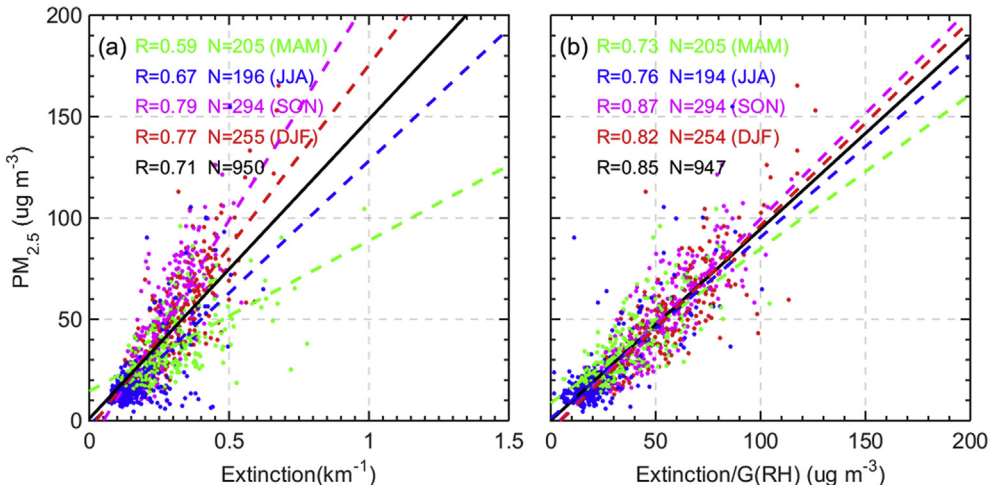
#### 4. Validation of satellite derived $PM_{2.5}$

Combining the two processes described in Section 3.1 and Section 3.2, we are able to derive surface-level concentration of  $PM_{2.5}$  from AOD. Since the climatology of extinction profiles and  $BLH_{lidar}$ ,  $BLH_{rs}$ , and  $BLH_{rd}$  can be respectively applied for estimating aerosol distributions, we consequently obtain four approaches for retrieving  $PM_{2.5}$ , and are referred to as "approach 1" (climatology), "approach 2" ( $BLH_{lidar}$ ), "approach 3" ( $BLH_{rs}$ ), and "approach 4" ( $BLH_{rd}$ ) respectively. It should be noted that approaches 2–4 use the same algorithm to convert AOD to  $PM_{2.5}$ . Our purpose is to

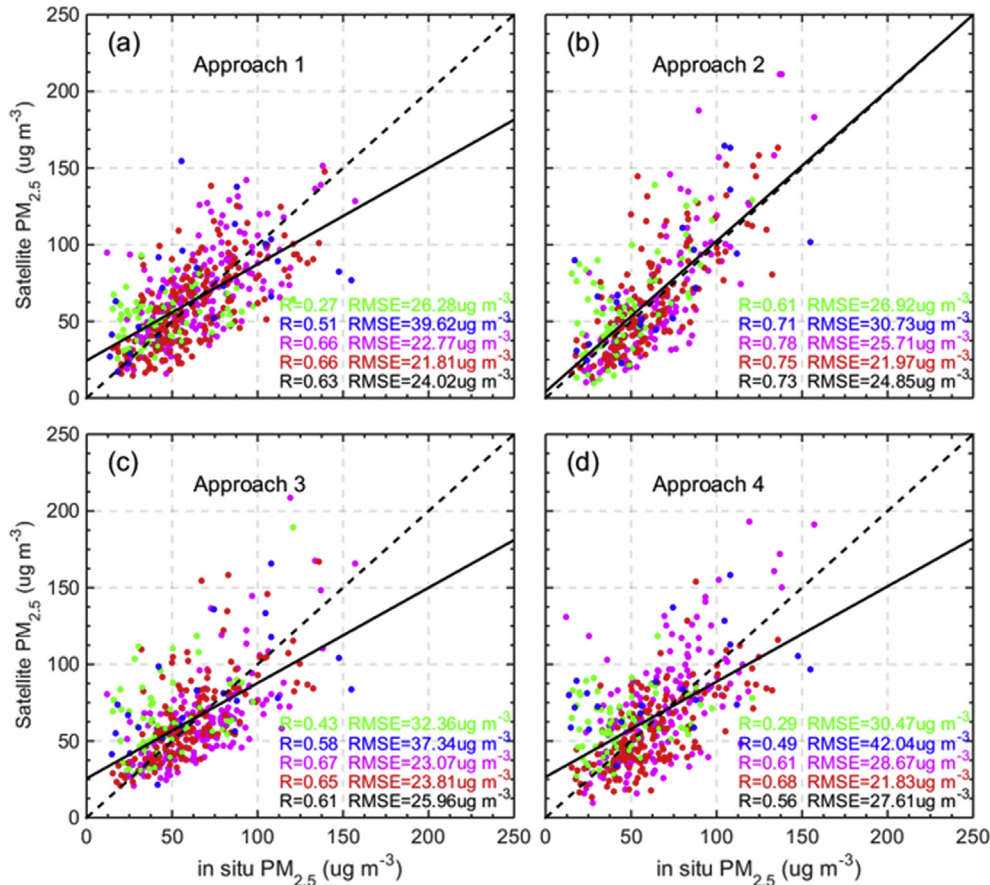
evaluate the effect of different BLH calculation methods. The extinction profiles derived from MPL accurately characterize the vertical distribution, but bear some uncertainties in the absolute value due to the uncertainties in the lidar ratio, which is difficult to quantify. Thus, we directly apply the four approaches of retrieving  $PM_{2.5}$  to MODIS AOD. We match the surface measurements of  $PM_{2.5}$ , RH, and BLHs to MODIS AOD. Since the  $PM_{2.5}$  and RH are hourly averaged, we interpolate these data to the exact overpass time of the satellites. Fig. 9 presents the seasonal scatter plots between  $PM_{2.5}$  concentrations derived from surface observation and those derived from satellites for different approaches.

Fig. 9 indicates that the correlations between satellite retrievals and in situ observations vary largely across different approaches. Approach 2 achieves the highest correlation of 0.73, while the correlation for approach 4 is only 0.56. Since the differences between approach 2–4 come from the different BLH retrievals, we present the comparisons of noontime BLHs derived from MPL, RS, and reanalysis data in Fig. 10. In general,  $BLH_{lidar}$  and  $BLH_{rs}$  agree well with each other, while the agreements between  $BLH_{lidar}$  and  $BLH_{rd}$  are worse. The differences in BLH products are closely related to their different definitions. The identification of  $BLH_{lidar}$  depends on the gradient of aerosol signal, and is thus strongly associated with aerosol vertical extent. Meanwhile,  $BLH_{rs}$  and  $BLH_{rd}$  are derived from potential temperature profile and turbulent fluxes respectively, which are related to thermodynamics conditions. Therefore,  $BLH_{lidar}$  usually identifies the top height of an aerosol-rich layer, while  $BLH_{rs}$  and  $BLH_{rd}$  do not necessarily represent the aerosol vertical structure. As a result, the accuracies of approaches 3–4 are lower than approach 2. The worst agreement is found between approach 4 and in situ observations, likely due to modeling uncertainties. For seasonal differences, the correlations are considerably lower for spring and summer. This is reasonable, since poorer performances have already been found for both the vertical and hydroscopic corrections. Root-mean-square errors (RMSE) are also much higher for spring and summer, where approaches 1 and 2 have lower, similar overall values.

Fig. 11 shows the distributions of the biases between observations and satellite retrievals of  $PM_{2.5}$ . The black and red dashed lines indicate the corresponding averaged biases and the averaged absolute biases respectively. Because clouds frequently occur within the  $10 \text{ km} \times 10 \text{ km}$  grids during spring and summer, the sample volumes for MODIS AOD are comparatively lower during these two seasons. Large overestimates are also noticed for approaches 2–4 in



**Fig. 8.** (a) Comparison between noontime  $PM_{2.5}$  and surface extinction for MAM (green), JJA (blue), SON (pink), DJF (red). (b) Comparison between noontime  $PM_{2.5}$  and extinction/ $G$ . The correlation coefficients ( $R$ ) and sample numbers ( $N$ ) are given in each panel.



**Fig. 9.** The comparison of PM<sub>2.5</sub> derived from surface observation and MODIS AOD for MAM (green), JJA (blue), SON (pink), DJF (red). Four approaches for estimating the vertical distribution of extinction are applied respectively. The correlation coefficients (R), RMSE for difference seasons and all are given in each panel.

spring and summer. As shown in Fig. 6, large amounts of elevated aerosols above the PBL can be observed during these two seasons, even accounting for more than 50% of the column AOD during spring. These non-negligible elevated aerosols would result in an overestimate of PM<sub>2.5</sub> using satellite retrievals. Meanwhile, the systematic biases are relatively low for approach 1, since this approach is derived from climatology patterns and takes into account the issue of elevated aerosols during different periods of a year. For approaches 2–3, the overestimations of satellite retrievals are 30–39% in spring, and are 18–35% in summer. For approach 1, the overestimations of satellite retrievals are less than 15% for each

season.

Similar seasonal patterns can be found for the absolute biases. The absolute biases vary from 29.7% to 34.9% with the lowest value in approach 1 and the highest value in approach 4. Still, the higher values are found in spring and summer for both averaged biases and averaged absolute biases. The averaged biases generally reach maxima in spring, while the averaged absolute biases are the highest in summer.

Approach 1 is fully based on empirical parameters. To further verify the applicability of these parameters, approach 1 is applied to MODIS AOD obtained at Yuen Long during 2010–2013. Here,

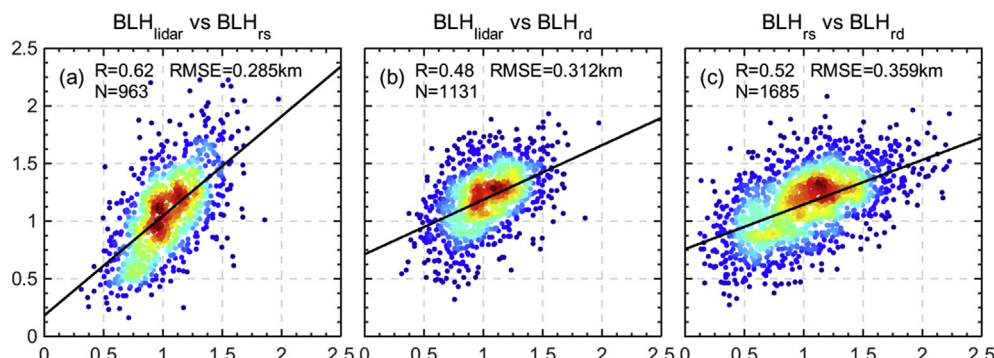


**Fig. 10.** The comparisons of noontime BLHs derived from MPL, radiosonde, and reanalysis data. The color-shaded dots indicate the normalized sample density. The correlation coefficients (R), RMSE, and sample numbers (N) are given in each panel.

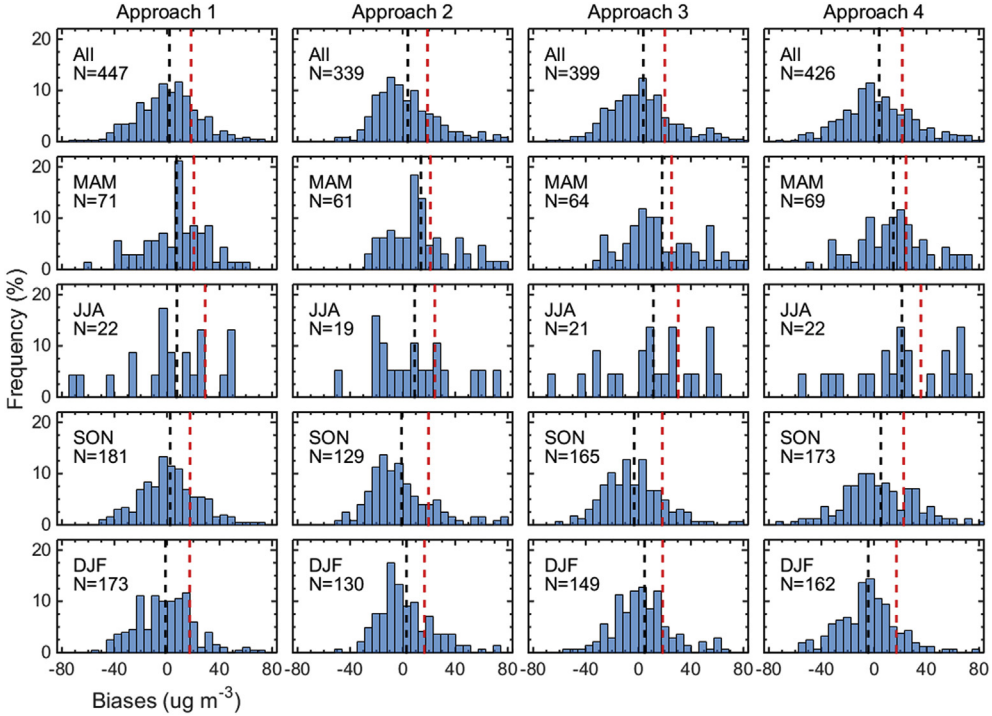


**Fig. 11.** Seasonal histogram of the biases of  $\text{PM}_{2.5}$  between surface observation and satellite retrievals for the four approaches. The black and red dashed lines indicate the averaged biases and the averaged absolute biases respectively. The sample numbers (N) are given in each panel.

approach 1 utilized the same climatology pattern shown in Fig. 3. Fig. 12 shows the good agreement for the updated comparison. Although the daily profiles vary largely, the statics pattern still can serve as a useful approach for determining the aerosol vertical distributions. It should also be noted that there are minor differences in the correlation coefficients for approach 1 during different periods. These differences may be caused by sampling biases, meteorological conditions, aerosols properties, etc.

## 5. Conclusions and discussion

In this study, we used different approaches for estimating aerosol vertical distribution to derive surface  $\text{PM}_{2.5}$  concentrations from columnar AOD measurements, and compared and evaluated their performances. In general, the AOD converted  $\text{PM}_{2.5}$  show reasonably good agreements with surface measurements for all four approaches. However, the detailed results can still vary considerably among different methods.

The approach of applying the climatology pattern of aerosol vertical distribution derived from MPL is originally developed in this study, which also exhibits good performance with the lowest biases. Compared with other empirical statistical regression methods, this approach effectively reduces the systematic biases in the retrievals since it accurately accounts for the portion of elevated aerosol during different periods. Our study also verifies that the climatology pattern of aerosol structure would be very useful for retrieving  $\text{PM}_{2.5}$ . For this approach, long-term historical data are required for constructing a representative climatology of aerosol vertical distribution. Since continuous lidar measurements are rare, space-borne lidar (e.g., CALIPSO) combined with ground-based observations and modeling offer great potential to construct large-scale aerosol vertical distribution climatologies (e.g. Tian et al., 2017).

Intercomparison between BLH retrieved using different measurement techniques and data sources suggests that the method for determining BLH is critical in deriving  $\text{PM}_{2.5}$ , and the agreements between observed and retrieved  $\text{PM}_{2.5}$  are highly variable for the use of different BLH products. Specifically, the MPL-derived BLHs are found to be the most suitable for retrieving  $\text{PM}_{2.5}$ , with a much higher correlation coefficient than the other two methods. The BLH derived from RS using the Holzworth method is also found to be suitable for retrieving  $\text{PM}_{2.5}$ , but has been largely ignored by previous research. Since the RS stations are widely distributed in China and routinely launched twice daily (Guo et al., 2016), there is a lot of

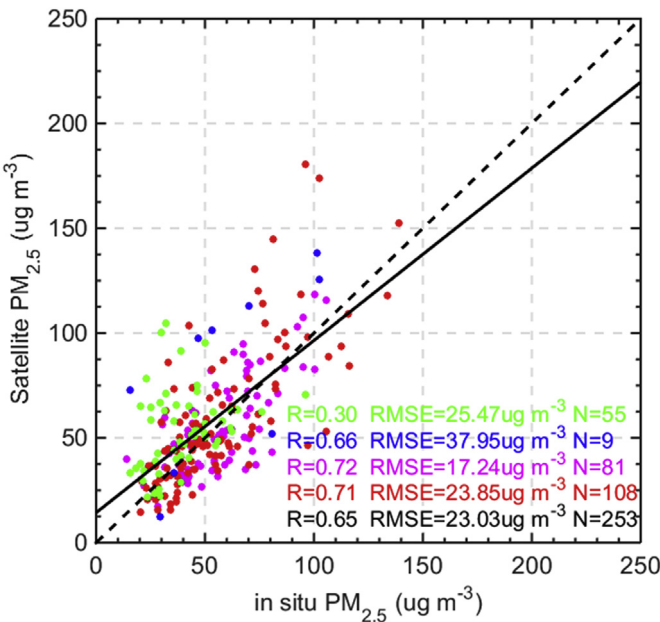


**Fig. 12.** The same as Fig. 9(a), but extends approach 1 to the MODIS AOD during 2010–2013.

potential for applying RS measurements for retrieving PM<sub>2.5</sub> from AOD. The BLHs derived from MERRA disagree with that from MPL and RS in terms of both the absolute value and the seasonality, and also exhibit the worst performance in estimating PM<sub>2.5</sub>. The unavoidable uncertainties in model simulations and BLH definition should be the main reason for this phenomenon.

In addition, the widely accepted assumptions about the aerosol vertical structure in retrieving PM<sub>2.5</sub> along with BLH are examined. For the homogenous assumption, since averaged extinctions in PBL agree well with surface extinction, this assumption can be considered valid during noontime. For the confinement assumption, however, it can be far from real situation. Actually, there are certain amounts of elevated aerosols above PBL, which can contribute up to ~40% of columnar AOD. Since the fraction of elevated aerosols is comparatively high in spring and summer, large uncertainties and overestimates of satellite retrievals are found for these two seasons. Our study implies that caution must be taken when using BLH to scale AOD in deriving PM concentration from column measurements.

For further studies, we plan to apply CALIPSO data along with ground-based observations to construct aerosol vertical distributions over a larger spatial scale. Such large-scale climatology of aerosol vertical structure will be beneficial for understanding the relationship between AOD and PM<sub>2.5</sub>. We also plan to further study the retrieval algorithms of BLH, as well as the role of BLH in retrieving PM<sub>2.5</sub>.

## Acknowledgements

The authors thank the MODIS team and NASA Langley data center for providing the AOD data used in this study. This study is funded by National Science Foundation of China (NSFC) (Grant No.: 41375008, 41575018 and 41175020).

## References

- Ackerman, A.S., Kirkpatrick, M.P., Stevens, D.E., Toon, O.B., 2004. The impact of humidity above stratiform clouds on indirect aerosol climate forcing. *Nature* 432 (7020), 1014–1017.
- Barnaba, F., Putaud, J.P., Gruening, C., Dos Santos, S., 2010. Annual cycle in co-located in situ, total-column, and height-resolved aerosol observations in the Po Valley (Italy): implications for ground-level particulate matter mass concentration estimation from remote sensing. *J. Geophys. Res. Atmos.* 115 (D19).
- Benas, N., Beloconi, A., Chrysoulakis, N., 2013. Estimation of urban PM10 concentration, based on MODIS and MERIS/AATSR synergistic observations. *Atmos. Environ.* 79, 448–454.
- Boers, R., Eloranta, E.W., Coulter, R.L., 1984. Lidar observations of mixed layer dynamics: tests of parameterized entrainment models of mixed layer growth rate. *J. Clim. Appl. Meteorol.* 23 (2), 247–266.
- Boucher, O., et al., 2013. Clouds and aerosols. In: Climate Change 2013: the Physical Science Basis. Contribution of Working Group I to the Fifth Assessment Report of the Intergovernmental Panel on Climate Change. Cambridge Univ. Press, Cambridge, U. K, pp. 571–657.
- Boyouk, N., Léon, J.F., Delbarre, H., Podvin, T., Deroo, C., 2010. Impact of the mixing boundary layer on the relationship between PM2.5 and aerosol optical thickness. *Atmos. Environ.* 44 (2), 271–277.
- Brunekreef, B., Forsberg, B., 2005. Epidemiological evidence of effects of coarse airborne particles on health. *Eur. Respir. J.* 26 (2), 309–318.
- Campbell, J.R., Reid, J.S., Westphal, D.L., Zhang, J., Tackett, J.L., Chew, B.N., Welton, E.J., Shimizu, A., Sugimoto, N., Aoki, K., et al., 2013. Characterizing the vertical profile of aerosol particle extinction and linear depolarization over Southeast Asia and the Maritime Continent: the 2007e2009 view from CALIOP. *Atmos. Res.* 122, 520e543.
- Carlton, A.G., Wiedinmyer, C., Kroll, J.H., 2009. A review of secondary organic aerosol (SOA) formation from isoprene. *Atmos. Chem. Phys.* 9 (14), 4987–5005.
- Chan, C.K., Yao, X., 2008. Air pollution in mega cities in China. *Atmos. Environ.* 42 (1), 1–42.
- Chu, D.A., Ferrare, R., Szykman, J., Lewis, J., Scarino, A., Hains, J., et al., 2015. Regional characteristics of the relationship between columnar AOD and surface PM<sub>2.5</sub>: application of lidar aerosol extinction profiles over Baltimore–Washington Corridor during DISCOVER-AQ. *Atmos. Environ.* 101, 338–349.
- Chu, D.A., Kaufman, Y.J., Zibordi, G., Chern, J.D., Mao, J., Li, C., et al., 2003. Global monitoring of air pollution over land from the Earth Observing System—Terra moderate resolution imaging spectroradiometer (MODIS). *J. Geophys. Res.* Atmos. 108 (D21). <http://dx.doi.org/10.1029/2002JD003179>.
- Cohn, S.A., Angevine, W.M., 2000. Boundary layer height and entrainment zone thickness measured by lidars and wind-profiling radars. *J. Appl. Meteorol.* 39 (8), 1233–1247.
- Dockery, D.W., Pope, C.A., Xu, X., Spengler, J.D., Ware, J.H., Fay, M.E., Ferris Jr., B.G., Speizer, F.E., 1993. An association between air pollution and mortality in six US cities. *N. Engl. J. Med.* 329 (24), 1753–1759.
- Drury, E., Jacob, D.J., Spurr, R.J., Wang, J., Shinouka, Y., Anderson, B.E., et al., 2010. Synthesis of satellite (MODIS), aircraft (ICARTT), and surface (IMPROVE, EPA-AQS, AERONET) aerosol observations over eastern North America to improve MODIS aerosol retrievals and constrain surface aerosol concentrations and sources. *J. Geophys. Res. Atmos.* 115 (D14). <http://dx.doi.org/10.1029/2009JD012629>.
- Du, C., Liu, S., Yu, X., Li, X., Chen, C., Peng, Y., Dong, Y., Dong, Z., Wang, F., 2013. Urban boundary layer height characteristics and relationship with particulate matter mass concentrations in Xi'an, central China. *Aerosol Air Qual. Res.* 13, 1598–1607.
- Engel-Cox, J., KimOanh, N.T., van Donkelaar, A., Martin, R.V., Zell, E., 2013. Toward the next generation of air quality monitoring: Particulate matter. *Atmos. Environ.* 80, 584–590.
- Fernald, F.G., 1984. Analysis of atmospheric lidar observations: some comments. *Appl. Optic.* 23 (5), 652–653.
- Flamant, C., Pelon, J., Flamant, P., 1997. Lidar determination of the entrainment zone thickness at the top of the unstable marine atmospheric boundary layer. *Bound. Layer Meteorol.* 83 (2), 247–284.
- Guo, J., Miao, Y., Zhang, Y., Liu, H., Li, Z., Zhang, W., He, J., Lou, M., Yan, Y., Bian, L., Zhai, P., 2016. The climatology of planetary boundary layer height in China derived from radiosonde and reanalysis data. *Atmos. Chem. Phys.* 16 (20), 13309–13319.
- Guo, J., Su, T., Li, Z., Miao, Y., Li, J., Liu, H., Xu, H., Cribb, M., Zhai, P., 2017. Declining summertime local-scale precipitation over eastern China from 1970 to 2010 and its potential link to aerosols. *Geophys. Res. Lett.* <http://dx.doi.org/10.1002/2017GL073533>.
- Guo, J., Zhang, X., Che, H., Gong, S., An, X., Cao, C., Guang, J., Zhang, H., Wang, Y., Zhang, X., Zhao, P., Li, X., 2009. Correlation between PM concentrations and aerosol optical depth in eastern China. *Atmos. Environ.* 43 (37), 5876–5886.
- He, Q., Li, C., Geng, F., Zhou, G., Gao, W., Yu, W., Li, Z., Du, M., 2016. A parameterization scheme of aerosol vertical distribution for surface-level visibility retrieval from satellite remote sensing. *Remote Sens. Environ.* 181, 1–13.
- He, Q.S., Li, C.C., Mao, J.T., Lau, A.K.H., Li, P.R., 2006. A study on the aerosol extinction-to-backscatter ratio with combination of micro-pulse LIDAR and MODIS over Hong Kong. *Atmos. Chem. Phys.* 6, 3243–e3256.
- Ho, K.F., Lee, S.C., Cao, J.J., Chow, J.C., Watson, J.G., Chan, C.K., 2006. Seasonal variations and mass closure analysis of particulate matter in Hong Kong. *Sci. Total Environ.* 355 (1), 276–287.
- Holzworth, G., 1964. Estimates of mean maximum mixing depths in the contiguous United States. *Mon. Weather Rev.* 92 (5), 235–242.
- Holzworth, G., 1967. Mixing depths, wind speeds and air pollution potential for selected locations in the United States. *J. Appl. Meteorol.* 6 (6), 1039–1044.
- Hooper, W.P., Eloranta, E.W., 1986. Lidar measurements of wind in the planetary boundary layer: the method, accuracy and results from joint measurements with radiosonde and kytoon. *J. Clim. Appl. Meteorol.* 25 (7), 990–1001.
- Jordan, N.S., Hoff, R.M., Bacmeister, J.T., 2010. Validation of Goddard Earth Observing System-version 5 MERRA planetary boundary layer heights using CALIPSO. *J. Geophys. Res. Atmos.* 115 (D24).
- Karimian, H., Li, Q., Li, C., Jin, L., Fan, J., Li, Y., 2016. An improved method for monitoring fine particulate matter mass concentrations via satellite remote sensing. *Aerosol Air Qual. Res.* 16 (4), 1081–1092.
- Kennedy, A.D., Dong, X., Xi, B., Xie, S., Zhang, Y., Chen, J., 2011. A comparison of MERRA and NARR reanalyses with the DOE ARM SGP data. *J. Clim.* 24 (17), 4541–4557.
- Kiehl, J.T., Briegleb, B.P., 1993. The relative roles of sulfate aerosols and greenhouse gases in climate forcing. *Science* 260 (5106), 311–314.
- Klett, J.D., 1985. Lidar inversion with variable backscatter/extinction ratios. *Appl. Optic.* 24 (11), 1638–1643.
- Koschmieder, H., 1926. Theorie der horizontalen Sichtweite. *Beitsaege Phys. Atmos.* 12, 33–55.
- Koelemeijer, R.B.A., Homan, C.D., Matthijssen, J., 2006. Comparison of spatial and temporal variations of aerosol optical thickness and particulate matter over Europe. *Atmos. Environ.* 40 (27), 5304–5315.
- Lai, L.W., 2015. Fine particulate matter events associated with synoptic weather patterns, long-range transport paths and mixing height in the Taipei Basin, Taiwan. *Atmos. Environ.* 113, 50–62.
- Lee, H.J., Liu, Y., Coull, B.A., Schwartz, J., Koutrakis, P., 2011. A novel calibration approach of MODIS AOD data to predict PM2.5 concentrations. *Atmos. Chem. Phys.* 11 (15), 7991–8002.
- Levy, R.C., Remer, L.A., Kleidman, R.G., Mattoo, S., Ichoku, C., Kahn, R., Eck, T.F., 2010. Global evaluation of the Collection 5 MODIS dark-target aerosol products over land. *Atmos. Chem. Phys.* 10 (21), 10399–10420. Vancouver.
- Li, C., Hsu, N.C., Tsay, S.C., 2011. A study on the potential applications of satellite data in air quality monitoring and forecasting. *Atmos. Environ.* 45 (22), 3663–3675.
- Li, C., Lau, A.H., Mao, J., Chu, D.A., 2005a. Retrieval, validation, and application of the 1-km aerosol optical depth from MODIS measurements over Hong Kong. *IEEE Trans. Geoscience Remote Sens.* 43 (11), 2650–2658.

- Li, C., Mao, J., Lau, A.K.-H., Yuan, Z.B., Wang, M.H., Liu, X.Y., 2005b. Application of MODIS satellite products on the air pollution research in Beijing. *Sci. China Ser. D* 48 (Suppl. II), 209–219.
- Li, C., Mao, J., Lau, K.-H.A., Chen, J.-C., Yuan, Z., Liu, X., Zhu, A., Liu, G., 2003. Characteristics of distribution and seasonal variation of aerosol optical depth in eastern China with MODIS products. *Chin. Sci. Bull.* 48, 2488–e2495.
- Li, J., Li, C., Zhao, C., Su, T., 2016. Changes in surface aerosol extinction trends over China during 1980–2013 inferred from quality-controlled visibility data. *Geophys. Res. Lett.* 43 (16), 8713–8719.
- Li, Y., Lin, C., Lau, A.K., Liao, C., Zhang, Y., Zeng, W., Li, C., Fung, J.C., Tse, T.K., 2015. Assessing long-term trend of particulate matter pollution in the Pearl River Delta region using satellite remote sensing. *Environ. Sci. Technol.* 49 (19), 11670–11678.
- Li, Z., Zhang, Y., Shao, J., Li, B., Hong, J., Liu, D., Li, D., Wei, P., Li, W., Li, L., Zhang, F., 2016. Remote sensing of atmospheric particulate mass of dry PM<sub>2.5</sub> near the ground: method validation using ground-based measurements. *Remote Sens. Environ.* 173, 59–68.
- Lin, C.Q., Li, C.C., Lau, A.K., Yuan, Z.B., Lu, X.C., Tse, K.T., et al., 2016. Assessment of satellite-based aerosol optical depth using continuous lidar observation. *Atmos. Environ.* 140, 273–282.
- Lin, C., Li, Y., Lau, A.K., Deng, X., Tim, K.T., Fung, J.C., Li, C., Li, Z., Lu, X., Zhang, X., Yu, Q., 2016. Estimation of long-term population exposure to PM<sub>2.5</sub> for dense urban areas using 1-km MODIS data. *Remote Sens. Environ.* 179, 13–22.
- Lin, C., Li, Y., Yuan, Z., Lau, A.K., Li, C., Fung, J.C., 2015. Using satellite remote sensing data to estimate the high-resolution distribution of ground-level PM<sub>2.5</sub>. *Remote Sens. Environ.* 156, 117–128.
- Liu, Y., Park, R.J., Jacob, D.J., Li, Q., Kilaru, V., Sarnat, J.A., 2004. Mapping annual mean ground-level PM<sub>2.5</sub> concentrations using multiangle imaging spectroradiometer aerosol optical thickness over the contiguous United States. *J. Geophys. Res. Atmos.* 109 (D22). <http://dx.doi.org/10.1029/2004JD005025>.
- Lu, X., Lin, C., Li, Y., Yao, T., Fung, J.C., Lau, A.K., 2017. Assessment of health burden caused by particulate matter in southern China using high-resolution satellite observation. *Environ. Int.* 98, 160–170.
- McGrath-Spangler, E.L., Denning, A.S., 2012. Estimates of North American summertime planetary boundary layer depths derived from space-borne lidar. *J. Geophys. Res. Atmos.* 117 (D15).
- Melfi, S.H., Spinharne, J.D., Chou, S.H., Palm, S.P., 1985. Lidar observations of vertically organized convection in the planetary boundary layer over the ocean. *J. Clim. Appl. Meteorol.* 24 (8), 806–821.
- Morille, Y., Haefelin, M., Drobinski, P., Pelon, J., 2007. STRAT: an automated algorithm to retrieve the vertical structure of the atmosphere from single-channel lidar data. *J. Atmos. Ocean. Technol.* 24 (5), 761–775.
- Platt, C.M., et al., 1994. The experimental cloud lidar pilot study (ECLIPS) for cloud-radiation research. *Bull. Am. Meteorol. Soc.* 75 (9), 1635–1654.
- Qin, Y.M., Li, Y.J., Wang, H., Lee, B.P.Y.L., Huang, D.D., Chan, C.K., 2016. Particulate matter (PM) episodes at a suburban site in Hong Kong: evolution of PM characteristics and role of photochemistry in secondary aerosol formation. *Atmos. Chem. Phys.* 16 (22), 14131–14145.
- Rienecker, M.M., et al., 2008. NASA GSFC Technical Report Series on Global Modeling and Data Assimilation. The GEOS-5 Data Assimilation System—documentation of Versions 5.0.1 and 5.1.0, vol. 27, p. 92. NASA/TM-2007-104606.
- Rienecker, M.M., et al., 2011. MERRA: NASA's Modern-Era retrospective analysis for research and applications. *J. Clim.* 24, 3624–3648. <http://dx.doi.org/10.1175/JCLI-D-11-00015.1>.
- Sayer, A.M., Hsu, N.C., Hsiao, T.C., Pantina, P., Kuo, F., Ou-Yang, C.F., Holben, B.N., Janjai, S., Chantara, S., Wang, S.H., Loftus, A.M., 2016. In-situ and remotely-sensed observations of biomass burning aerosols at Doi Ang Khang, Thailand during 7-SEAS/BASELInE 2015. *Aerosol Air Qual. Res.* 16, 2786–2801.
- Schäfer, K., Harbusch, A., Emeis, S., Koepke, P., Wiegner, M., 2008. Correlation of aerosol mass near the ground with aerosol optical depth during two seasons in Munich. *Atmos. Environ.* 42 (18), 4036–4046.
- Seibert, P., Beyrich, F., Gryning, S.E., Joffre, S., Rasmussen, A., Tercier, P., 2000. Review and intercomparison of operational methods for the determination of the mixing height. *Atmos. Environ.* 34, 1001–1027. [http://dx.doi.org/10.1016/S1352-2310\(99\)00349-0](http://dx.doi.org/10.1016/S1352-2310(99)00349-0).
- Su, T., Li, J., Li, J., Li, C., Chu, Y., Zhao, Y., Guo, J., Yu, Y., Wang, L., 2017a. The evolution of springtime water vapor over Beijing observed by a high dynamic Raman Lidar system: case studies. *IEEE J. Sel. Top. Appl. Earth Obs. Remote Sens.* <http://dx.doi.org/10.1109/JSTARS.2017.2653811>.
- Su, T., Li, J., Li, C., Xiang, P., Lau, A.K.H., Guo, J., Yang, D., Miao, Y., 2017b. An inter-comparison of long-term planetary boundary layer heights retrieved from CALIPSO, ground-based lidar and radiosonde measurements over Hong Kong. *J. Geophys. Res. Atmos.* 122 <http://dx.doi.org/10.1002/2016JD025937>.
- Tao, M., Chen, L., Wang, Z., Tao, J., Che, H., Wang, X., Wang, Y., 2015. Comparison and evaluation of the MODIS Collection 6 aerosol data in China. *J. Geophys. Res. Atmos.* 120 (14), 6992–7005.
- Tian, P., Cao, X., Zhang, L., Sun, N., Sun, L., Logan, T., Shi, J., Wang, Y., Ji, Y., Lin, Y., Huang, Z., 2017. Aerosol vertical distribution and optical properties over China from long-term satellite and ground-based remote sensing. *Atmos. Chem. Phys.* 17 (4), 2509–2523.
- van Donkelaar, A., Martin, R.V., Pasch, A.N., Szykman, J.J., Zhang, L., Wang, Y.X., et al., 2012. Improving the accuracy of daily satellite-derived ground-level fine aerosol concentration estimates for North America. *Environ. Sci. Technol.* 46 (21), 11971–11978.
- van Donkelaar, A., Martin, R.V., Park, R.J., 2006. Estimating ground-level PM<sub>2.5</sub> using aerosol optical depth determined from satellite remote sensing. *J. Geophys. Res. Atmos.* 111 (D21).
- Wang, J., Christopher, S.A., 2003. Intercomparison between satellite-derived aerosol optical thickness and PM<sub>2.5</sub> mass: implications for air quality studies. *Geophys. Res. Lett.* 30 (21). <http://dx.doi.org/10.1029/2003GL018174>.
- Wang, Z., Chen, L., Tao, J., Liu, Y., Hu, X., Tao, M., 2014. An empirical method of RH correction for satellite estimation of ground-level PM concentrations. *Atmos. Environ.* 95, 71–81.
- Wang, Z., Chen, L., Tao, J., Zhang, Y., Su, L., 2010. Satellite-based estimation of regional particulate matter (PM) in Beijing using vertical-and-RH correcting method. *Remote Sens. Environ.* 114, 50e63.
- Wiegner, M., Emeis, S., Freudenthaler, V., Heese, B., Junkermann, W., Münkel, C., Schäfer, K., Seefeldner, M., Vogt, S., 2006. Mixing layer height over Munich, Germany: variability and comparisons of different methodologies. *J. Geophys. Res.* 111 (D13), 1–17. <http://dx.doi.org/10.1029/2005JD006593>.
- Wu, Y., Guo, J., Zhang, X., Tian, X., Zhang, J., Wang, Y., Duan, J., Li, X., 2012. Synergy of satellite and ground based observations in estimation of particulate matter in eastern China. *Sci. Total Environ.* 433, 20–30.
- Yang, D.W., Li, C., Lau, A.K.-H., Li, Y., 2013. Long-term measurement of daytime atmospheric mixing layer height over Hong Kong. *J. Geophys. Res. Atmos.* 118, 2422–2433. <http://dx.doi.org/10.1002/jgrd.50251>.
- Zhang, Y., Li, Z., 2015. Remote sensing of atmospheric fine particulate matter (PM<sub>2.5</sub>) mass concentration near the ground from satellite observation. *Remote Sens. Environ.* 160, 252–262.
- Zhang, Y., Gao, Z., Li, D., Li, Y., Zhang, N., Zhao, X., Chen, J., 2014. On the computation of planetary boundary-layer height using the bulk Richardson number method. *Geosci. Model Dev.* 7 (6), 2599–2611.
- Zheng, J., Zhang, L., Che, W., Zheng, Z., Yin, S., 2009. A highly resolved temporal and spatial air pollutant emission inventory for the Pearl River Delta region, China and its uncertainty assessment. *Atmos. Environ.* 43 (32), 5112–5122.